AIAA JOURNAL
Vol. 41, No. 11, November 2003

Technical Notes

TECHNICAL NOTES are short manuscripts describing new developments or important results of a preliminary nature. These Notes cannot exceed six manuscript pages and three figures; a page of text may be substituted for a figure and vice versa. After informal review by the editors, they may be published within a few months of the date of receipt. Style requirements are the same as for regular contributions (see inside back cover).

Dynamic Loading Methodologies

Monty A. Moshier* and Ronald L. Hinrichsen†
RHAMM Technologies, Bellbrook, Ohio 45305
and
Gregory J. Czarnecki‡
U.S. Air Force Research Laboratory, Wright–Patterson Air Force Base, Ohio 45433

Introduction

In live-fire testing of aircraft wings, quasi-static ground loading techniques do not account for changes in structural stiffness and mass that occur during damage infliction. As such, current loading methodologies do not reconfigure to correctly represent in-flight loads. In addition, ground loading methodologies fail to consider damage-induced changes to the flutter envelope that can lead to premature failure. A reconfigurable ground loading methodology or dynamic loading methodology (DLM) is envisioned that takes into account a wing's change in stiffness. In addition, an analytical procedure is required that considers a wing's damage state and predicts a revised flutter envelope. The new ground loading procedure and complimentary flutter analysis will support live-fire testing and assist in the generation of reliable and complete test assessments and vulnerability analyses.

A strategy has been postulated for accomplishing a reconfigurable ground loading methodology wherein modeling and simulation techniques play an important role. The following step-by-step process summarizes the strategy:

1) Obtain and/or build a validated finite element structural model and couple it with an aerodynamic flow model.

2) Perform a time-integrated finite element simulation of the aircraft in flight. During the simulation, at $t = 0$ apply the g loading and aerodynamic loading to the model.

3) At a time when the model is at or near steady state ($t = t_1$), instantaneously inflict damage (equivalent to a specific threat) by removing structural elements from the model.

4) Monitor the time history of displacements and strains at specific points in the model.

5) Design a ground loading system to mimic the model response for the 1–2 s following the damage.

General Model Details

A finite element structural model was obtained of a representative fighter aircraft in NASTRAN format. This model had been previously validated for use in dynamic analysis and optimization. The NASTRAN model was translated into the LSDYNA3D keyword format using a combination of preprocessors and user-written translation codes. Figure 1 shows a view of the resulting finite element model. The finite element model consisted of beams, shells, and lumped masses and inertias. Because the focus of this work was on the wing, the highest fidelity elements were used there while other structures were modeled with less fidelity. The fuselage, vertical, and horizontal tails are essentially beam models. The structural model consisted of 4226 nodes, 2016 beam elements, 4984 shell elements, and 998 lumped masses and inertias.

The aerodynamic paneling model was a boundary element method based on the VSAERO code.[1] Because it is based on linear aerodynamic theory, it is applicable for inviscid, incompressible fluid flows. Figure 2 shows the aerodynamic model used in this sample case.

This aeromodel is the result of a convergence study performed to obtain the optimum aeromodel refinement. It consists of 336 elements using nodes that are coincident with and numbered the same as the structural model nodes. By imposing the coincidence of the aero- and structural nodes, pressures generated by the aeromodel are directly applied to the structural nodes.

After the NASTRAN finite element model of the structure was converted to LSDYNA3D format, it was necessary to revalidate the model. This was done by comparing the performance of the two models against existing data that had been obtained from earlier static and dynamic ground tests.

During the static ground test, the aircraft wing was cantilevered horizontally from a strong back wall and subjected to a static load at buttline (B.L.) 120. Displacement measurements at the loading points were taken. Comparisons of model predictions of the displacements with those obtained during the test are shown in Fig. 3.

For this comparison, the wing model was detached from the fuselage model and cantilevered to replicate boundary conditions of the ground test. The aerodynamic model was replaced with a concentrated line load at B.L.120. Because LSDYNA3D is an explicit time-integration code, results are plotted in the time domain. The

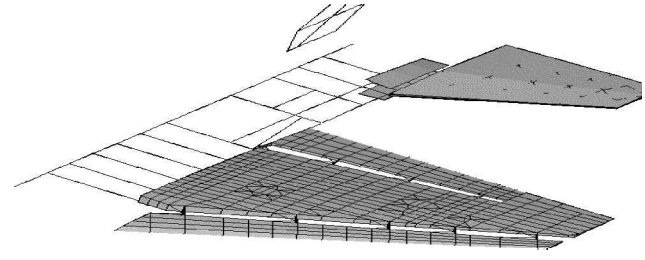

Fig. 1 Structural model.

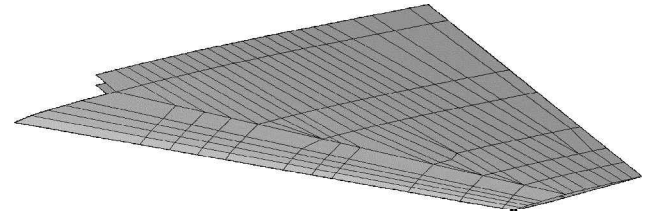

Fig. 2 Aerodynamic panel model.

Presented as Paper 2002-1492 at the AIAA/ASME/ASCE/AHS/ASC 43rd Structures, Structural Dynamics, and Materials Conference, Denver, CO, 22–25 April 2002; received 20 March 2003; revision received 1 August 2003; accepted for publication 1 August 2003.

*Senior Scientist, 332 Skyland Drive. Member AIAA.
†Chief Scientist, 332 Skyland Drive. Senior Member AIAA.
‡Aerospace Engineer, 2700 D Street, B1661 R228, 46th Test Wing.

Table 1 Natural frequency comparison

Mode	Ground test, Hz	LSDYNA3 D model, Hz	NASTRAN model, Hz (Ref. 2)
1	11.39	9.61	10.03
2	34.76	31.20	26.97
3	36.51	32.60	32.99
4	56.16	53.00	41.44

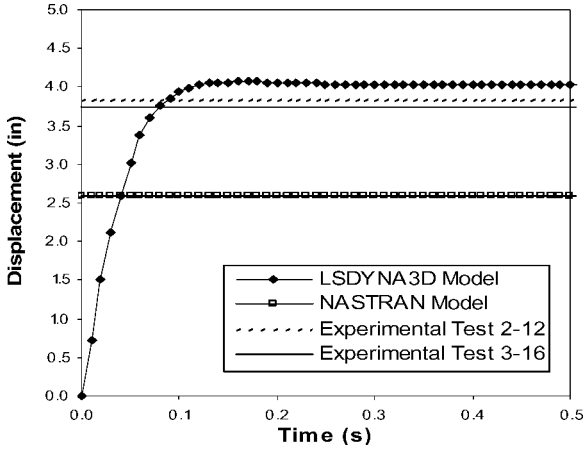

Fig. 3 Aerodynamic panel model.

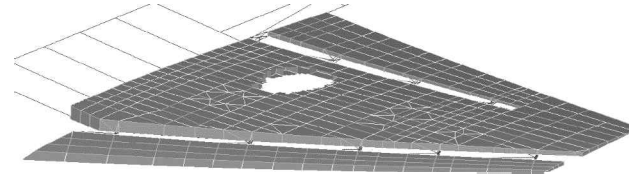

Fig. 4 Typical damages: Mach 0.80.

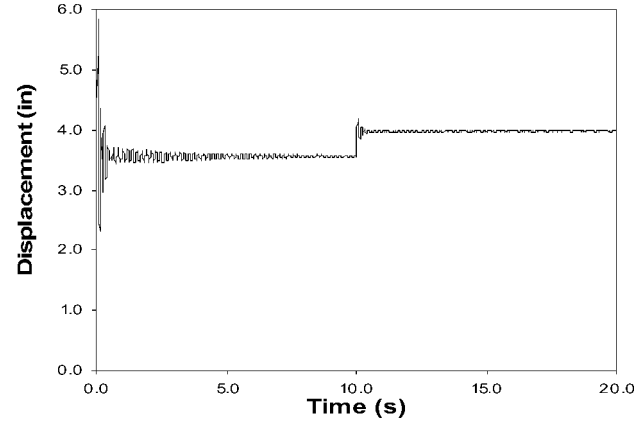

Fig. 5 Deflection at B.L. 120 for a clean wing and typical damage: Mach 0.80.

smooth buildup of displacement vs time of the LSDYNA3D model is the result of a ramped loading in combination with damping.

One can see from Fig. 3 that the LSDYNA3D model predicts a displacement approximately 5% greater than ground test. One striking observation is that when compared to the original NASTRAN model[2] the LSDYNA3D model is significantly better. The model displacement is quite sensitive to the position of the cantilevered boundary condition. Additional refinement of that boundary condition would have led to closer agreement, but it was decided that the 5% difference was acceptable.

During the dynamic ground test, the aircraft wing was cantilevered vertically from a strong back, instrumented, and subjected to a ground vibration/modal analysis test. Table 1 shows the comparison of natural frequencies between the LSDYNA3D and NASTRAN models with the experimental data. The difference between the LSDYNA3D model and the ground test values varies between 6 and 16%.

Dynamic Response Due to Damage

The dynamic response of a damaged wing is primarily a result of the reduced stiffness caused by the damage. More important is the wing's loss of resistance to flutter, or the reduction in the flutter speed capability of the wing due to damage. A damaged wing can survive and the aircraft can continue to fly if 1) static stiffness is sufficient to withstand the aerodynamic loads (this assumes that sufficient lifting capability is still present) and 2) damage does not reduce the flutter speed such that the wing responds in a manner wherein it uncontrollably flutters and destroys itself.

To better understand the dynamic response of the wing when subjected to damage, it was determined that several different conditions must be considered. Because of the nature and use of fighter aircraft, this study evaluated the effect of different stores, flight conditions, damage locations, and size. Over 68 cases were investigated, of which only 2 are highlighted here. The stores that were investigated ranged in weight from 200 to 2000 lb (0.89 to 8.9 kN). Flight conditions ranged from Mach 0.8 to 0.95 below altitudes of 4000 ft (1219 m). Damage included three different damage sites and two different damage sizes.

The results presented here are from simulations in which the wing was undamaged for the first 10 s with instantaneous damage to the wing occurring at $t = 10$ s followed by an additional 10 s of simulation. The aerodynamic paneling method used in LSDYNA3D does not currently allow for ramping up of the aerodynamic flow. Because of this, the initial 10 s of simulation are required to allow the wing's response to the step loading due to the aerodynamic flow to reach a steady state. Instantaneous damage to the wing at $t = 10$ s is achieved by removing elements associated with the assumed damage. The resulting dynamic response due to the damage and applied aerodynamic loading is then captured in the final 10 s of the simulation. The aerodynamic mesh does not change throughout the simulation.

Sample Case 1

Case 1 investigates the dynamic response of a clean wing damaged near the wing root with moderate damage (Fig. 4). The model simulation was for the aircraft at an angle of attack of 6 deg, altitude below 4000 ft (1219 m), and Mach 0.8.

This particular case illustrates the structural redundancy of this wing. After the wing reaches steady state, aerodynamic loading causes the undamaged wing to deflect approximately 3.5 in. (0.089 m), as measured from B.L.120 (Fig. 5). Figure 5 also shows that once damage occurs the instantaneous loss of structural stiffness initiates some brief oscillations followed by a steady-state deflection that is approximately 0.5 in. (0.0127 m) more than the predamage state. The stress contour plots for this case are uninteresting because stresses in the wing before and after damage are below the yield stress of the materials used.

Under these simulated flight conditions, the wing's loss of flutter resistance due to damage does not affect the dynamic response of the wing sufficiently to cause catastrophic failure. However, brief oscillations experienced immediately following damage, under the right conditions, may cause additional damage that results in additional flutter resistance loss. It is important to note that the models in this investigation used linear elastic material behavior and that additional failure modes are not included.

The redundancy of this wing can be demonstrated by looking at stresses in the damaged spar caps. Figure 6 shows spar cap stresses in spar caps 6 and 7 before and after damage. Portions of spar caps 7, 8, 9, and 10 are eliminated at time $t = 10$ s. Before damage is input, spar caps 6 and 7 are loaded to about -12 ksi (82.7 mPa). After damage, spar cap 6 is loaded to -30 ksi (206.8 mPa) because it carries additional load from the damaged spar caps. The yield stress of aluminum used in modeling the spar caps is 70 ksi (482.6 mPa). As can be seen from Fig. 6, the postdamage stresses are far below the allowable yield.

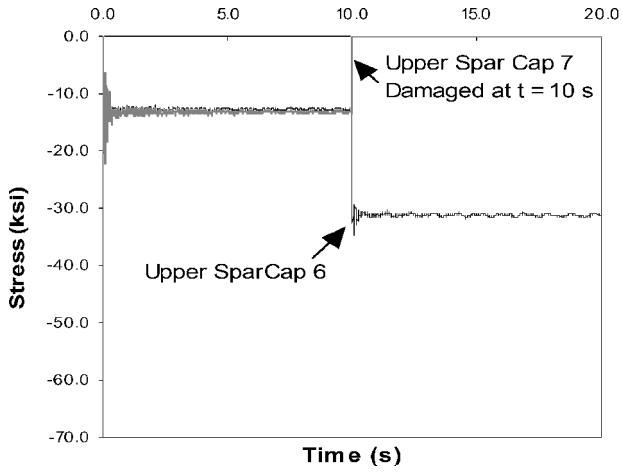

Fig. 6 Spar cap stresses before and after damage.

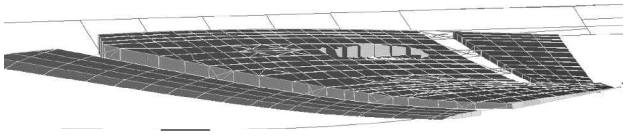

Fig. 7 Wing deflection with typical damage and wing tip store: Mach 0.92.

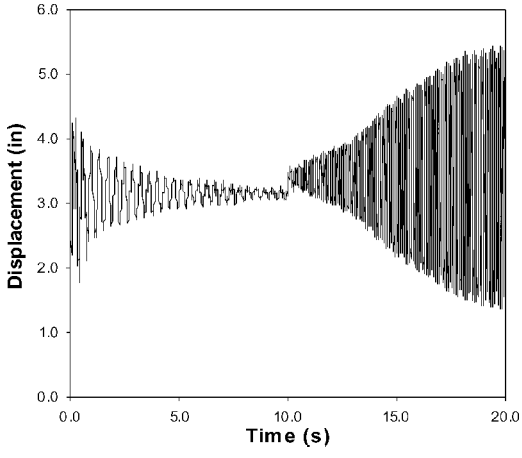

Fig. 8 Deflection at B.L. 120 for wing + 300-lb (1334.5-N) store and typical damage: Mach 0.92.

Sample Case 2

In case 2, a 300-lb (1334.5-N) store was attached to the wing tip and the dynamic response was investigated when the wing was again damaged near the wing root (Fig. 7). This case used an angle of attack of 3 deg, altitude below 4000 ft (1219 m), and Mach 0.92. As can be seen in Fig. 8, the store was modeled as a series of simple beams. Figure 7 also shows the wing's deflection and tortuous shape caused by the damage and loss of flutter resistance.

Oscillations associated with step loading the wing at the beginning of the simulation require more time to reach steady state than the previous case (Fig. 8). Additionally, after damage the deflection diverges due to the lower stiffness and reduced flutter speed.

The reduced flutter resistance caused by the damage led to increased deflections resulting in stresses that exceed the allowable yield stresses of the materials used. Figure 9a shows the von Mises stresses for the wing prior to damage, where the von Mises stresses are scaled such that black is 0 ksi and gray 70 ksi (482.6 mPa), corresponding to the maximum allowable yield stress. Prior to damage the von Mises stresses were all well below the yield stresses. However, after damage and due to the increased deflections caused by flutter, von Mises stresses exceeded the allowable yield stress in the entire tip region (Fig. 9b). The likely result would be the loss of the wing tip and possible loss of the aircraft.

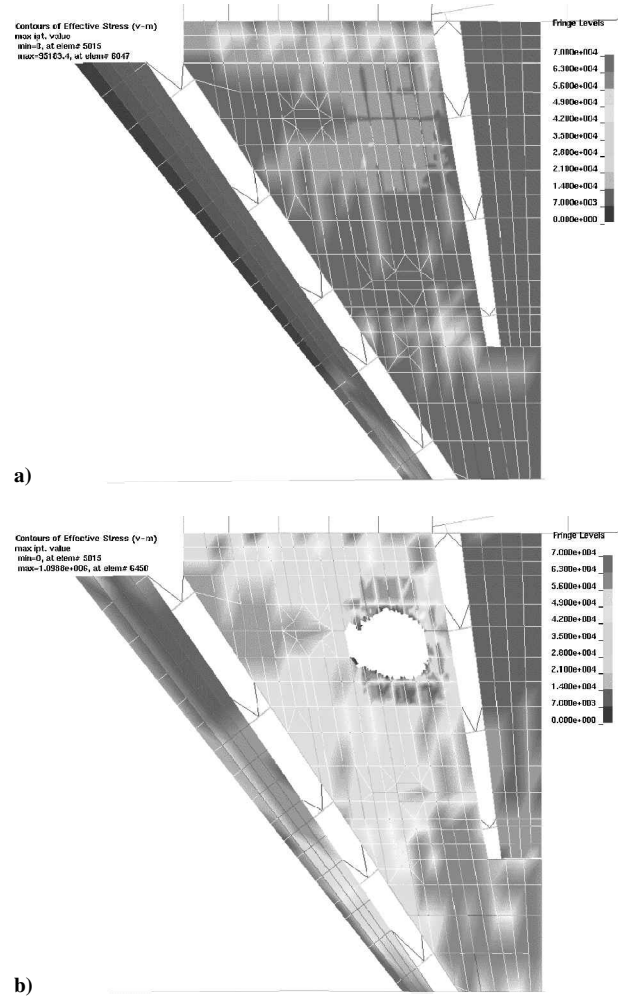

Fig. 9 Von Mises stress contour plot for wing a) before and b) after damage.

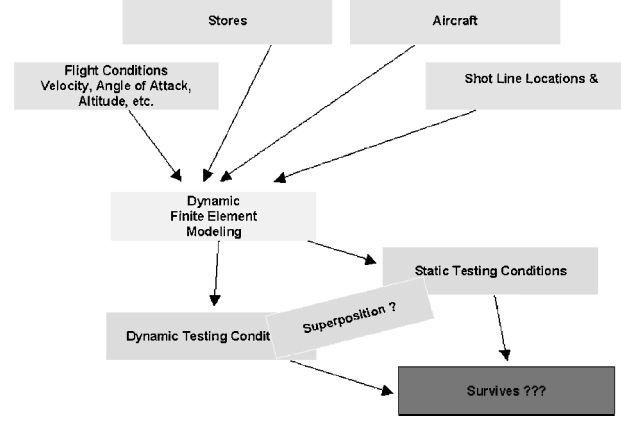

Fig. 10 Proposed dynamic loading methodology strategy.

Conclusions

In this Note, the authors presented a strategy that the DLM team is pursuing to more faithfully represent aircraft structural response to damage inflicted in flight. The strategy is based on a validated, coupled, aerodynamic/structural finite element model.

The modeling that was performed in this study illustrated the complexity of different conditions that must be addressed before an assessment regarding survivability can be made. The decision process must first start with a list of known factors and conditions. These required factors and conditions include aircraft selection, stores, fuel load, flight conditions, shot location, threat selection, and so on.

It is clear that modeling plays a key roll in determining appropriate loading methods for a determination of aircraft survivability. The proposed methodology uses dynamic finite element techniques to determine the dynamic response of selected aircraft undergoing an in-flight change of stiffness. Results of the dynamic analysis provide a pathway to the test engineer for determining the most appropriate test method. That method could either be static, dynamic, or a combination of the two (Fig. 10).

The team is currently investigating possible pneumatic, hydraulic, or combined loading techniques that could be used to apply dynamic loads during ground tests. It is anticipated that experimental ground testing can be applied for cases similar to case 1. The simulations have shown that the dynamic response and flutter resistance based on cases similar to that of case 2 result in deflections that, if applied to an actual wing, would lead to structural failure. Therefore, when flutter plays a key role in the dynamic response of the wing due to damage (case 2), it is anticipated that computational analyses will be used as the primary tool for accurately assessing postdamage survivability. Furthermore, it is important to note that a full structural evaluation should account for more than just a maximum yield stress criterion as was done here. Many other failure mechanisms from plasticity to cracking must also be considered.

References

[1]Maskew, B., "Program VSAERO Theory Document," NASA CR-4023, 1987.

[2]Negaard, G. R., "Finite Element Analysis of Ballistic Tests," U.S. Air Force Wright Aeronautical Lab., AFWAL-TR-88-3041, Wright–Patterson AFB, OH, 1988.

A. Palazotto
Associate Editor

Sound Waveform Effect on Disturbance Generation in Turbulent Jets at Aeroacoustic Interaction

V. G. Pimshtein*
Central Aerohydrodynamic Institute, 107005, Moscow, Russia

Introduction

AMONG a large number of the papers devoted to sound interaction with turbulent jets, the works associated with investigations of the spectral composition of the acoustic excitation affecting the disturbance generation and development in jets, aerodynamic jet parameters, and noise radiation occupy a significant place.[1] Usually the effect of different spectra of the acoustic excitation is considered in such works, particularly the effect of separate spectral components on the aeroacoustic interaction process, mainly on the process of vortex coupling, if the case in point is subsonic jets. As a rule in such cases, the important role of the fundamental tone subharmonic, as the component affecting this process and resulting from it, is emphasized. Though it is known that the excitation spectrum and the process time dependency should cause one another, the effect of the sound waveform itself on the process of aeroacoustic interaction usually is not taken into account. Sokolov et al.[2] presented some evidence that the form of the sound wave can substantially affect the coherent structure initiation, and Vlasov et al.[3] studied the sound waveform effect on low-speed (up to 20 m/s) jet spreading. However, the average aerodynamic characteristics, which do not allow for a definition of details of the aeroacoustic interaction mechanism, were measured in these works.

Received 29 April 2002; revision received 15 May 2003; accepted for publication 20 May 2003.

*Senior Research Scientist, Acoustic Division, 17 Radio Str.

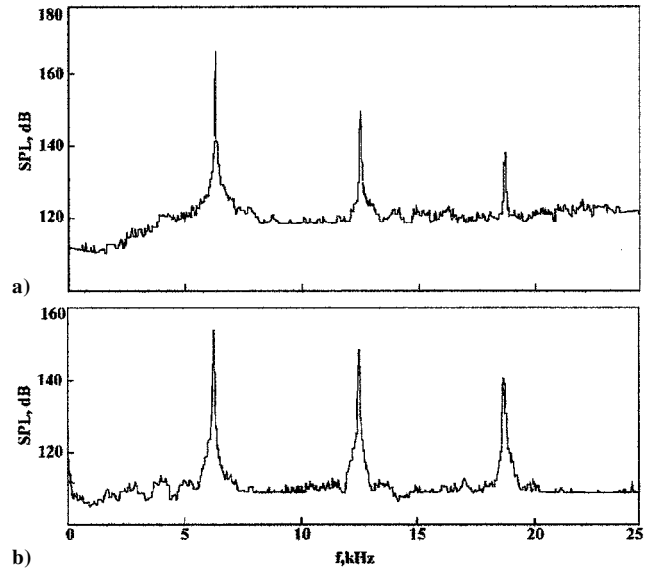

Fig. 1 Sound pressure spectra at different distances from the HG in frequency bands Δf = 32 Hz, f = 6.3 kHz: $-l$ = a) 5 and b) 150 mm.

The purpose of this Note is to investigate the sound waveform effect on coherent structure generation in subsonic and supersonic turbulent jets under lateral high-intensity excitation by sinusoidal and sawtoothlike waves.

The experiments were carried out in a large anechoic chamber of the Acoustic Division of the Central Aerohydrodynamic Institute with unheated subsonic ($\bar{p}_o = 1.4$) and underexpanded supersonic air jets issuing from convergent nozzle ($M = 1.0$, $\bar{p}_o = 3.4$–3.7) and a supersonic jet issuing from the convergent–divergent nozzle ($M = 2.0$, $\bar{p}_o = 6.2$) with exit diameter $d = 20$ mm. (Here $\bar{p}_o = p_o/p_a$ is the pressure ratio at the nozzle, p_o is the total pressure in the settling chamber of the nozzle, p_a is the ambient pressure, and M is the nozzle design Mach number.) Hartman generators (HGs) with a frequency of 4.0–8.5 kHz were used as the sound sources. The sinusoidal high-intensity sound wave near the generator becomes enriched with higher harmonics during its propagation and is transformed into a sawtoothlike wave. This circumstance was used in the experiments: Fig. 1 presents sound pressure spectra at different distances from the generator. Acoustic measurements (rms value of the sound pressure) were carried out with a Bruel and Kjaer microphone (model 4136) located near the nozzle edge and a Bruel and Kjaer spectrometer (model 2032), where the accuracy of the data obtained is ±1 dB. At small distances from the sound source ($l = 5$–10 mm) the sound wave is almost sinusoidal: the fundamental tone level exceeds the first harmonic by 15–20 dB (Fig. 1a). At large distances (100–150 mm) the difference between the levels of the fundamental and highest harmonics decreases (Fig. 1b) and the sinusoidal wave transforms into a sawtoothlike one. The sound pressure level (SPL) at the nozzle lip with sinusoidal excitation was 165 dB and for excitation by a sawtoothlike sound wave it was 155–170 dB. An SPL of 170 dB was achieved using sound reflectors. Visualization of jets, coherent structures, and sound waves was carried out with a direct shadowgraph technique with a spark source (the size of a luminous body of 0.8 mm and exposure time 2×10^{-7} s). It should be noted, however, that because the direct shadowgraph technique used is the most sensitive to the second derivative of intensity, sinusoidal sound waves cannot be seen in shadow pictures even at rather high sound intensity.

Results and Discussion

Figure 2 presents typical photographs of the subsonic jet ($\bar{p}_o = 1.4$) excited by a sinusoidal high-intensity sound wave (Fig. 2a; $f = 4.0$ kHz, SPL = 165 dB), by a sawtoothlike sound